

The impact of topographically-forced stationary waves on the local ice sheet climate

Johan Liakka,¹ Johan Nilsson¹

¹*Department of Meteorology, S-106 91 Stockholm, Sweden*

E-mail: liakka@misu.su.se

ABSTRACT. A linear two-level atmospheric model is employed to study the influence of ice sheet topography on the atmospheric stationary waves. In particular, the stationary wave-induced temperature anomaly is considered locally over a single ice sheet topography, which is computed using the plastic approximation. It is found that the stationary waves induce a local cooling which increases linearly with the ice volume for ice sheets of horizontal extents smaller than about 1400 km. Beyond this horizontal scale, the dependence of the stationary wave-induced cooling on the ice volume becomes gradually weaker. For a certain ice sheet size, and for small changes of the surface zonal wind, it is further shown that the strength of the local stationary wave-induced cooling is proportional to the basic state meridional temperature gradient times the vertical stratification in the atmosphere. These results are of importance for the nature of the feedback between ice sheets and the stationary waves, and may also serve as a basis for parameterising this feedback in ice sheet model simulations, e.g. through the Pleistocene glacial-interglacial cycles.

INTRODUCTION

At the Last Glacial Maximum (LGM; about 18-20 kyr ago) the Northern Hemisphere was occupied by two major ice sheets which both are absent today; the Laurentide ice sheet over North America and the Eurasian ice sheet. The LGM extents of these ice sheets are well constrained by observational data (Clark and Mix, 2002; Dyke, 2004), whereas their evolution to their maximum extents remains unconstrained (Dyke and others, 2002; Kleman and others, 2002). In

25 addition to the orbital variations of the Earth (Milankovitch, 1930; Berger, 1978), feedbacks between the ice sheets and
26 their environment must be taken into account when considering the evolution of the ice sheets through the last glacial-
27 interglacial cycle. A number of early studies have shown that the high albedo and the elevation of the ice sheets are
28 important feedbacks that further support ice growth (e.g. Weertman, 1976; Källén and others, 1979; Oerlemans, 1980).
29 Furthermore, the ice sheets constitute topographic barriers, which influence the midlatitude atmospheric circulation
30 (Kutzbach and Guetter, 1986; Cook and Held, 1988; Kageyama and Valdes, 2000; Justino and others, 2005; Abe-Ouchi
31 and others, 2007). In turn, the changes in the circulation patterns may alter the temperature and precipitation fields over
32 the ice sheets themselves (Oerlemans, 1979; Lindeman and Oerlemans, 1987; Hall and others, 1996; Roe and Lindzen,
33 2001a,b). Some studies even suggest that variations in the orbital parameters influence the atmospheric circulation,
34 which may be an important mechanism supporting the onset of the Northern Hemisphere glaciations (Kageyama and
35 others, 2004; Cubasch and others, 2006; Otiño and Bromwich, 2009). The presence of ice sheets may also shift the
36 precipitation pattern to an increased dominance of upslope precipitation (Sanberg and Oerlemans, 1983; Roe, 2005; van
37 den Berg and others, 2008).

38 Several studies have successfully simulated the last glacial-interglacial cycle in reasonable accord with observational
39 data (e.g. Pollard, 1982; Tarasov and Peltier, 1997; Paillard, 1998; Tarasov and Peltier, 2004; Bonelli and others, 2009).
40 However, uncertainties associated with e.g. ice dynamics, basal sliding and the atmospheric state still remain. Simulations
41 of the last glacial-interglacial cycle using a dynamical ice sheet model forced by climatology computed by Atmospheric
42 General Circulation Models (AGCM:s) have shown to be sensitive to the atmospheric state (Abe-Ouchi and others,
43 2007; Charbit and others, 2007). In the study of Charbit and others (2007) it was found that the simulated ice volumes
44 and spatial extents of the ice sheets were highly dependent on the AGCM that was used to force the ice sheet model.
45 Depending on the AGCM, the difference in terms of simulated ice volume in the Northern Hemisphere at LGM was at
46 most $30 \times 10^{15} \text{ m}^3$, which amounts to more than half of the estimated ice-equivalent sea level reduction at LGM.

47 While the influence of the albedo and ice-elevation feedbacks on the surface mass balance (SMB) of an ice sheet are
48 relatively straight forward, the feedbacks from the atmospheric circulation may be more complex. Variations of the zonal
49 mean wind have an impact on the amplitude and phase of the temperature anomalies induced by the topographically-
50 forced stationary waves due to the presence of an ice sheet (Hoskins and Karoly, 1981; Held, 1983). This may have an
51 impact also on the SMB of the ice sheet. An illuminating study on this subject was made by Roe and Lindzen (2001b),
52 who examined how a single ice sheet on an idealised continent evolved from a regional-scale initial size to a continental-
53 scale equilibrium size using a coupled stationary wave-ice sheet model. Their study suggests that the features of the ice
54 sheet at equilibrium are strongly shaped by temperature anomalies created by topographically-forced stationary waves,

55 which served to increase its equilibrium extent. Roe and Lindzen primarily focused on how the interactions between
56 the stationary waves and the ice sheet affected its equilibrium features. Given the rather complex dependence of the
57 stationary wave-induced temperature anomalies over the ice sheet on its spatial structure, however, the nature of the
58 feedback between the stationary waves and ice sheet topography may vary qualitatively throughout the evolution of the
59 ice sheet.

60 In this study, we examine the stationary wave response to changes in ice sheet topography in a linear, steady, quasi-
61 geostrophic two-level model. We have deliberately chosen a highly idealised atmospheric model and a plastic ice sheet
62 topography to allow for qualitative analyses and analytical solutions of the stationary wave response over a broad range
63 of parameters. The emphasis of this study is on the influence of ice sheet topography on the local stationary wave-
64 induced temperature anomalies, rather than on the fully-coupled interactions between the stationary waves and the ice
65 sheets that was addressed by Roe and Lindzen (2001b). The present study, which does not encompass any surface mass
66 balance calculations for the ice sheets, aims to derive relations for the stationary wave-induced temperature anomalies
67 over ice sheets that can serve as a basis to parameterize the stationary wave feedback in ice sheet models: One central
68 result is that the mean stationary wave-induced cooling over the ice sheet increases linearly with ice volume for small-
69 to-intermediate sized ice sheets. In the context of a one-dimensional ice sheet model, Roe and Lindzen (2001a) proposed
70 that the stationary wave-induced temperature anomaly should be proportional to the maximum height of the ice sheet.
71 Our results suggest that a near linear dependence of the temperature anomaly on the ice volume is appropriate for a
72 two-dimensional ice sheet; for a one-dimensional ice sheet we obtain a near linear dependence on the ice volume per
73 unit width.

74 **MODEL FORMULATION AND BOUNDARY CONDITIONS**

75 **Ice sheet topography**

The ice sheet profile is calculated under the assumption of perfect plasticity (van der Veen, 1999). As a result of the
plastic approximation, the ice sheet deforms instantly when the applied stress exceeds a critical value given by the yield
stress τ_0 . This implies that the stress within the ice sheet never exceeds the yield stress and that the ice thickness can
be related to its horizontal extent; here measured by the half-length of the ice sheet, L , in both horizontal directions.
The assumption of perfect plasticity, which is a first-order approximation of ice sheet topography, has been successfully
used in previous studies for obtaining analytical expressions of the ice sheet-climate interactions (e.g. Weertman, 1976;
Källén and others, 1979). Accounting for local isostatic depression, the maximum height of the ice sheet surface η_0 and

the maximum ice thickness H_0 are related to the horizontal extent as:

$$\eta_0 = \left(\frac{\sigma}{1 + \zeta} L \right)^{1/2}, \quad (1)$$

$$H_0 = (1 + \zeta)\eta_0. \quad (2)$$

76 Here, $\sigma \equiv 2\tau_0/(\rho_i g)$ relates the height of the ice sheet to its length-scale, and $\zeta \equiv \rho_i/(\rho_m - \rho_i)$ yields the bedrock
 77 depression, where ρ_i is the ice density, ρ_m the mantle density and g the gravitational acceleration. For each gridpoint,
 78 the height of the ice sheet surface is given by:

$$\eta(x, y) = \eta_0 A(x_d) A(y_d), \quad (3)$$

where x_d and y_d represent the distance from the centre of the ice sheet to x and y , respectively, and:

$$A(p) = (1 - |p/L|)^{1/2}, \text{ if } |p/L| \leq 1, \quad (4)$$

$$A(p) = 0, \text{ if } |p/L| > 1$$

79 where p is center distance. Finally, the total ice-volume V is given by:

$$V = 4L^2 H_m = 4L^2 (1 + \zeta) \eta_m = \frac{16}{9} (1 + \zeta)^{1/2} \sigma^{1/2} L^{5/2}, \quad (5)$$

80 where H_m and η_m represent the mean ice thickness and height of the ice surface, respectively. Integrating Eq. (3) from
 81 0 to L in both the x and y directions, it is easily shown that $(H_m, \eta_m) = 4/9(H_0, \eta_0)$.

82 Stationary wave model

83 The atmospheric response to ice sheet topography is examined in a linear two-level quasi-geostrophic model on a β -
 84 plane channel. The model is schematically outlined in Fig. 1. It should be underlined that the two-level model is highly
 85 idealised, but has been widely used in the past as it enables analytical solutions. The rationale for choosing a linear
 86 model with topographic forcing is partly based on the results obtained by Cook and Held (1988), who suggested that
 87 the winter stationary-wave pattern over North America at LGM was primarily a linear response to topographic forcing.
 88 Unfortunately, the linear model is unable to resolve interactions between ice sheets and transient waves acting on
 89 synoptic time-scales (3-7 days). Topographically-forced changes of these waves can influence both the precipitation and
 90 the temperature variability, two features that could have a significant impact on the ice sheet mass balance. In Cartesian
 91 coordinates, using the rigid-lid approximation, the barotropic and baroclinic stream function anomalies (ψ_M and ψ_T)
 92 of the linear quasi-geostrophic two-level model take the following form:

$$\left(\frac{\partial}{\partial t} + U_M \frac{\partial}{\partial x} \right) \nabla^2 \psi_M + \beta_0 \frac{\partial \psi_M}{\partial x} + U_T \frac{\partial}{\partial x} \nabla^2 \psi_T$$

$$= -\frac{f_0}{H}(U_M - U_T)\eta \quad (6)$$

$$\begin{aligned} & \left(\frac{\partial}{\partial t} + U_M \frac{\partial}{\partial x} \right) \left(\nabla^2 \psi_T - 2L_d^{-2} \psi_T \right) + \beta_0 \frac{\partial \psi_T}{\partial x} + U_T \frac{\partial}{\partial x} \left(\nabla^2 \psi_M + 2\psi_M L_d^{-2} \right) \\ & = \frac{f_0}{H} (U_M - U_T) \eta, \end{aligned} \quad (7)$$

where $\eta(x, y)$ is the height to the ice sheet surface, x and y are the Cartesian coordinates in the zonal and meridional directions, respectively. Equations (6) and (7) are identical to Eqs. (8.15) and (8.16) in Holton (2004) except for the surface topography terms on the right-hand sides of our equations. These terms enter the equations through the lower boundary condition of the vertical velocity w , which is non-zero in our case due the non-flat surface. The remaining notations of Eqs. (6) and (7) include the Laplace operator ∇^2 , the geometric model depth H , the Coriolis parameter f_0 , and β_0 , which is the meridional gradient of f_0 . Both f_0 and β_0 are calculated at 50°N . The exact choice of this latitude does not change the conclusions of this study. The Rossby radius of deformation, L_d , is given by:

$$L_d = \frac{NH}{2f_0}, \quad (8)$$

where $N = \sqrt{(g/\theta)(\partial\theta/\partial z)}$ is the Brunt-Väisälä frequency (θ is the potential temperature). Hence the value of L_d increases with the vertical stability of the atmosphere. The subscripts M and T denote barotropic and baroclinic quantities, respectively, and are related to each model level as:

$$a_M = \frac{a_1 + a_2}{2} \quad \text{Barotropic} \quad (9)$$

$$a_T = \frac{a_1 - a_2}{2} \quad \text{Baroclinic}, \quad (10)$$

where a is an arbitrary variable, and the notations 1 and 2 denote the upper and lower model levels, respectively. Using these notations, U_M is the vertically averaged zonal mean wind, and U_T is the thermal wind (i.e. the vertical wind shear scaled by 2.) Both U_M and U_T are spatially uniform and related to the corresponding stream function through the geostrophic approximation.

Because the time-scale of ice sheet expansion is much longer than that of the atmosphere, we neglect the local time derivatives in Eqs. (6) and (7). The resulting steady-state barotropic and baroclinic equations are then given by:

$$\begin{aligned} & U_M \frac{\partial}{\partial x} \nabla^2 \psi_M + \beta_0 \frac{\partial \psi_M}{\partial x} + U_T \frac{\partial}{\partial x} \nabla^2 \psi_T \\ & = -\frac{f_0}{H} (U_M - U_T) \eta - \frac{1}{2\tau_F} \nabla^2 (\psi_M - \psi_T) \end{aligned} \quad (11)$$

$$U_M \frac{\partial}{\partial x} \left(\nabla^2 \psi_T - 2L_d^{-2} \psi_T \right) + \beta_0 \frac{\partial \psi_T}{\partial x} + U_T \frac{\partial}{\partial x} \left(\nabla^2 \psi_M + 2L_d^{-2} \psi_M \right)$$

$$= \frac{f_0}{H}(U_M - U_T)\eta + \frac{1}{2\tau_F}\nabla^2(\psi_M - \psi_T) - \frac{2}{\tau_T}L_d^{-2}\psi_T. \quad (12)$$

111 A typical feature of the linear quasi-geostrophic steady-state equations (11) and (12) is the occurrence of a resonance
 112 singularity at the critical stationary zonal wavenumber, which depends mainly on the zonal mean wind (Held, 1983). The
 113 singularity, which gives rise to an infinite stream function response, is removed by adding linear damping on vorticity
 114 with the damping time-scale τ_F to the lower model equation. To the baroclinic equation (12), we have also included
 115 radiative damping, which relaxes the topographically-forced temperature anomalies towards a zonal mean state with
 116 the time-scale τ_T .

117 Through the hydrostatic equation, the temperature anomaly at the 500 hPa level, T' , is given by:

$$T' = \frac{2f_0\psi_T}{R}, \quad (13)$$

118 where R is the gas constant for dry air. The background meridional temperature gradient, \overline{T}_y , is given by thermal wind
 119 relation as:

$$\overline{T}_y = -\frac{2f_0U_T}{R}. \quad (14)$$

120 We assume that U_M and U_T are related to each other as $U_T = 0.4U_M$, which is in rough agreement with the annual-mean
 121 present-day climate in the mid-latitudes in the Northern Hemisphere (Peixoto and Oort, 1992). The equations above
 122 are solved using standard Fast Fourier Transforms on a domain which is periodic in the x-direction (here interpreted as
 123 longitude). In the meridional direction, the boundary conditions $\psi_M = 0$ and $\psi_T = 0$ are applied at 90°N and at 0° . We
 124 use 512 gridpoints in both horizontal directions.

125 **Experimental design**

126 The boundary condition of the two-level model is represented by a single ice sheet. Due to the periodic nature of the
 127 atmospheric model in the zonal direction, the east-west location of the ice sheet is irrelevant. The northern margin of
 128 the ice sheet is chosen to be fixed at $y_N = 75^\circ\text{N}$, implying that the position of the southern margin is determined by
 129 the ice sheet half-length L .

130 To calculate atmospheric temperature anomalies of reasonable amplitude in the two-level model, we need to assign a
 131 proper atmospheric basic state, which is determined by the zonal mean wind U_M , the vertical wind shear U_T , and the
 132 deformation radius L_d . Because the basic state in a glacial climate is not precisely known, we need to find combinations
 133 of U_M , U_T and L_d that seem physically reasonable. To proceed, we consider the following two atmospheric basic states:

134 Present-day basic state: $U_M = 9 \text{ m s}^{-1}$; $U_T = 3.6 \text{ m s}^{-1}$; $L_d = 700 \text{ km}$

135 Glacial basic state: $U_M = 12 \text{ m s}^{-1}$; $U_T = 4.8 \text{ m s}^{-1}$; $L_d = 810 \text{ km}$

136 Roughly, the present-day state represents annual-mean present-day conditions in the mid-to-high latitudes in the North-
137 ern Hemisphere. The annual variations of the basic state parameters at these latitudes are quite small; the jet stream is
138 weaker in the summer but compensated by a northward shift (Peixoto and Oort, 1992). Because most ablation occurs
139 in the summer months, the stationary wave influence on the local ice sheet climate should be interpreted as the summer
140 response. The glacial basic state is calculated using a stronger background meridional temperature gradient. This is a
141 rough estimate of the atmospheric conditions during periods with extensive ice sheets on the Northern Hemisphere, e.g.
142 at LGM (see e.g. Cook and Held, 1988). The value of L_d for both states is calculated under the assumption that the
143 atmospheric state, on longer time-scales, is near the critical shear of baroclinic instability, which is given by $2U_T = \beta_0 L_d^{-2}$
144 (Stone, 1978). The maximum amplitude of the stationary wave-induced temperature over a continental-scale ice sheet
145 of similar extent to the Laurentide ice sheet at LGM amounts to -4.7°C for the present-day basic state and to -5.7°C
146 for the glacial basic state, which is in the same order of magnitude as simulated by Roe and Lindzen (2001b).

147 Due to the sparse vertical resolution of the two-level model, the temperature anomalies computed at the 500 hPa level
148 (around 6 km height) should be interpreted as temperature anomalies at the ice sheet surface, which at most reaches
149 an elevation of 3.7 km in this study. Due to the uncertainties associated with the meridional distribution of the local
150 temperature anomaly in channel models, we use the ice sheet area-averaged temperature anomaly $\overline{T'}$ to monitor the net
151 stationary wave influence on the temperature over the ice sheet. Finally, the numerical values of the parameters used in
152 this study are given in Table 1.

153 **THE SCALE-DEPENDENT INTERACTION BETWEEN ICE SHEETS AND STATIONARY** 154 **WAVES**

155 Here, we analyse qualitatively how temperature and snow-fall anomalies forced by the ice sheet can affect its mass
156 balance and evolution. In particular, we examine the scale dependence of effects that either act to change the ice volume
157 or act to reorganize the ice sheet structure. Conceptually, the rate of changes of the surface height of an ice sheet
158 can be expressed as:

$$\frac{\partial \eta}{\partial t} = f(T_s, w, \eta, \nabla \eta, \dots). \quad (15)$$

159 Here, the mass-balance function f contains all processes that locally affect the height of the ice sheet, including accumu-
160 lation, ablation, and ice dynamics. Note that for a perfectly plastic ice sheet, the shape and the volume are independent
161 of the local mass balance. However, in this conceptual analysis we allow for departures from the perfect plastic behaviour

162 that enforces a parabolic ice-sheet profile. To analyse qualitatively the interaction between the stationary waves and the
 163 ice sheet, we assume that the stationary wave-induced temperature anomaly T' and the topographically-forced vertical
 164 velocity w give rise to small perturbations on the surface mass balance of an ice sheet that is essentially in equilibrium,
 165 i.e. $f \approx 0$. Hence, we crudely approximate Eq. (15) as:

$$\frac{\partial \eta}{\partial t} = -pT' + qw, \quad (16)$$

166 where $p \equiv -\partial f / \partial T_s$ and $q \equiv \partial f / \partial w$ are positive constants converting the temperature anomaly and the vertical velocity
 167 to actual mass balance. The rationale for Eq. (16) is that we assume that the temperature anomalies primarily influence
 168 the surface mass balance via ablation (Roe and Lindzen, 2001a,b) and that the accumulation increases with vertical
 169 velocity, resulting in enhanced upslope precipitation (Sanberg and Oerlemans, 1983; Roe and Lindzen, 2001b). In reality,
 170 also the accumulation can be influenced by the stationary wave-induced temperature anomalies, an effect that for the
 171 sake of simplicity is omitted here. Note that the simplistic temperature dependence of the ablation in Eq. (16) assumes
 172 some pre-existing ablation, which a small temperature perturbation may either enhance or reduce. Essentially, $T' > 0$
 173 implies ice-elevation decrease due to enhanced melting, whereas $T' < 0$ implies ice-elevation increase due to reduced
 174 melting.

175 The isolated effect of our crude representation of topographically-induced snow fall is to move the ice sheet upwind:
 176 Using the fact that $w = U_2(\partial \eta / \partial x)$ in Eq. (16), we obtain the advection equation $\partial \eta / \partial t - q \cdot U_2(\partial \eta / \partial x) = 0$, describing
 177 a shape preserving upwind translation of the ice sheet. Note that this simple linear accumulation formula has no net
 178 effect on the ice sheet mass balance. In reality, the topographically-induced snow fall is a non-linear function of the
 179 vertical velocity and tends generally to enhance the accumulation over an ice sheet (see e.g. Sanberg and Oerlemans,
 180 1983; Roe and Lindzen, 2001b). We can crudely estimate the implied upwind translation speed $q \cdot U_2$ resulting from
 181 the accumulation formula of Roe and Lindzen (2001b); see their Fig. 4. By linearizing this formula around $w = 0$ and
 182 taking the surface temperature to be at the freezing point, we obtain $q \approx 1.5 \cdot 10^{-6}$. For a surface wind speed of 5 m
 183 s^{-1} , the upwind translation speed is found to be about 250 m per year. Thus, this crude consideration suggests that
 184 topographically-induced snow fall can induce a tendency of the ice sheets to move upwind with a speed a few 100 meters
 185 per years.

186 To examine the effect on the ice sheet of the simple ablation representation in Eq. (16), we set $q = 0$, and consider a
 187 single Fourier component of the ice sheet and the forced response:

$$(\psi_M, \psi_T, T', \eta) = (\tilde{\psi}_M(t), \tilde{\psi}_T(t), \tilde{T}(t), \tilde{\eta}(t)) e^{ikx} \sin ly. \quad (17)$$

188 Here k and l are the zonal and meridional wavenumbers, respectively. The time t is associated with the growth and
 189 decay of the ice sheet, which is much longer than the time-scale of the atmosphere. Inserting Eq. (17) into Eqs. (11)
 190 and (12), multiplying by i/k , and using Eq. (13), we obtain after some algebra (see the Appendix for details):

$$\tilde{T} = -\mu\chi\tilde{\eta}, \quad (18)$$

191 where $\mu \equiv 4f_0^2(U_M - U_T)/RH$. The function $\chi(k, l)$ relates the Fourier component of the ice sheet to the corresponding
 192 temperature anomaly; the analytical expression for this function is given in the Appendix. Substituting Eqs. (18) into
 193 (16) yields:

$$\frac{\partial \tilde{\eta}}{\partial t} = p\mu\chi\tilde{\eta}, \quad (19)$$

194 which have solutions on the form:

$$\tilde{\eta} = \exp(p\mu\chi t) \quad (20)$$

195 Because p and μ are positive constants, Fourier components for which $\text{Re}(\chi) > 0$ experience a positive feedback from
 196 the ablation anomalies; in the absence of stabilizing feedbacks they would grow exponentially. Wavenumbers for which
 197 $\text{Re}(\chi) < 0$, on the other hand, tend to decay. For a hypothetical infinite ice sheet characterised by a single Fourier compo-
 198 nent, $\text{Re}(\chi) > 0$ would correspond to a situation with cold/warm temperature anomalies at the ice sheet crests/throughs.
 199 The associated pattern of decreased and increased ablation would act to increase the amplitude of the sinusoidal ice
 200 sheet wave.

201 The quantity $p\mu\text{Im}(\chi)$ can be interpreted as the frequency of the ice sheet Fourier components, implying that the
 202 associated phase velocity in the zonal direction is given by:

$$c_p = -p\mu \frac{\text{Im}(\chi)}{k}, \quad (21)$$

203 and the zonal group velocity given by:

$$c_g = -p\mu \frac{\partial \text{Im}(\chi)}{\partial k}. \quad (22)$$

204 For a hypothetical sinusoidal ice sheet, $\text{Im}(\chi) < 0$ implies cold temperature anomalies and hence reduced ablation on
 205 the eastern (leeward) side of the crests; on the western (windward) side of the crests the opposite is true. This ablation
 206 pattern would act to advance the ice sheet eastward, i.e. inducing an eastward phase velocity. Hence, the phase shift
 207 between the ice sheet and the temperature anomalies, determined by $\text{Im}(\chi)$, affects the spatial evolution of the ice sheet
 208 but not its volume.

209 The scale-dependent interactions between the ice sheet and the stationary wave-induced temperature anomalies are
210 illustrated in Fig. 2, which shows the real and the imaginary part of $\chi(k, l)$. As a response to the ablation anomalies,
211 low as well as high ice sheet wavenumbers tend to be amplified, whereas intermediate ones tend to be attenuated; see Fig.
212 2a. The positive interval of the low wavenumbers terminates at the wavenumber of the stationary equivalent barotropic
213 Rossby wave (say K_s ; grey lines in Fig. 2), beyond which an interval with negative wavenumbers is encountered. The
214 stationary Rossby waves tend to dominate the atmospheric response (Charney and Eliassen, 1949; Held, 1983). When
215 $U_T = 0$, the wavenumber of the stationary Rossby wave is $K_s \equiv (k_s^2 + l_s^2)^{1/2} = (\beta_0 U_M^{-1})^{1/2}$; for typical atmospheric values
216 of U_T and L_d , K_s is slightly smaller. Note that it is for length scales comparable to the stationary wave that the ice
217 sheet experiences the strongest growth due to the stationary wave-induced ablation. The shift from cold temperature
218 anomalies to warm ones at k_s is essentially a barotropic phenomena; an analogous transition from negative to positive
219 stream-function response occurs in a barotropic model. The shift back to cold temperature anomalies (i.e. $\text{Re}(\chi) > 0$)
220 at higher wavenumbers occurs when zonal advection of relative vorticity begins to dominate.

221 The phase shift of the stationary wave-induced temperature anomalies, determined by $\text{Im}(\chi)$, results in an eastward
222 downstream advancement of the phase for all wavenumbers; see Eq. (21) and Fig. 2. This results from enhanced melting
223 due to warm anomalies on the upstream side and reduced melting due to cold anomalies on downstream side of the
224 ice sheet crests, which is the typical barotropic stationary-wave response over a topographic barrier (Held, 1983).
225 Further, Fig. 2 reveals that the group velocity can be downstream as well as upstream depending on the wavenumber.
226 The strongest growing wavenumbers, encountered near the wavenumber of the stationary Rossby wave, have a down-
227 stream group velocity. This tendency of downwind advancement due to ablation will compete with the effect due to
228 topographically-induced snow fall, which acts to advance the ice sheet upwind.

229 Earlier, we estimated that topographically-induced snow fall can advance an ice sheet upwind at a speed of a couple
230 of 100 meters per year and further noted that this speed is independent of the wavenumber. We now attempt a rough
231 estimate of the downwind phase speed of the ice sheet caused by the ablation anomalies due to the stationary waves.
232 For this purpose we use the ablation formula presented by Roe and Lindzen (2001a), which yields $p = 1.2 \text{ m yr}^{-1}$
233 $^{\circ}\text{C}^{-1}$. Substituting this value into Eq. (21), the phase speeds of the ice sheet wavenumbers are found to be between
234 5 and 15 km per year for the largest scales ($k < 6$), and approaching zero for smaller scales (not shown). This crude
235 analysis suggests that the ablation-induced phase speeds of long waves, which are directed downwind, can be an order
236 of magnitude greater than the upwind phase speed that is induced by upslope snow fall. This very crude estimate of
237 the ablation-induced phase speeds should be on the high side because it assumes some background ablation everywhere

238 over the ice sheet all year round. Thus, if for instance ablation occurs during a quarter of the year, the phase speeds
 239 would be reduced by 25 %.

240 THE INFLUENCE OF ICE VOLUME ON THE LOCAL STATIONARY WAVE-INDUCED 241 TEMPERATURE ANOMALY

242 In the previous section, we found that different scales of the stationary waves, described by the function χ , act to either
 243 enhance or reduce ice sheet ablation. In this section, we consider how the shape and volume of the ice sheet influence the
 244 local stationary wave-induced temperature response. The plastic nature of the ice sheets are exploited in the analysis.

245 Figure 3 shows the stationary wave-induced temperature anomaly, averaged over the ice sheet as a function of the
 246 ice volume. The temperature in Fig. 3 is non-dimensionalized by the multiplication of $(\bar{T}_y L_d)^{-1}$. In addition to the
 247 present-day and glacial basic states, we have included two additional simulations with different values of L_d ; these are
 248 illustrated by the grey lines in Fig. 3. Because the deformation radius L_d is associated with the vertical stratification in
 249 the atmosphere (cf. Eq. (8)), these additional simulations serve to illustrate the sensitivity to changes of the lapse rate
 250 in the glacial atmosphere, an issue that is still uncertain for LGM (Abe-Ouchi and others, 2007). The larger value of
 251 L_d corresponds to a strongly stratified atmosphere, implying a smaller lapse rate. Equivalently, the smaller value of L_d
 252 corresponds to a larger lapse rate. The scaled stationary wave-induced temperature exhibits nearly the same response for
 253 all basic states in Fig. 3. This means that the scaled temperature anomaly is insensitive to changes of the basic state,
 254 provided that the surface zonal wind, which is proportional to the temperature anomaly (see Eq. (18)), remains roughly
 255 constant.

256 To further examine the temperature anomaly changes with ice volume in Fig. 3, we consider the ice sheet Fourier
 257 components (see Eq. (18)). To begin with, it is illustrative to consider a general ice sheet formulation, defined as:

$$\eta = \eta_0 \eta_*(x/L, y/L). \quad (23)$$

258 Here, η_0 is the maximum height of the ice sheet surface. The extent of the ice sheet is constrained by its half-length L ,
 259 and its shape is given by η_* . In the zonal direction, the Fourier coefficients of Eq. (23) are given by:

$$\tilde{\eta}(k_n) = \eta_0 \frac{4}{R_e} \int_0^L \cos(k_n x) \eta_*(x/L) dx, \quad (24)$$

260 where R_e is the circumference around the Earth at a certain latitude and $k_n = 2\pi n/R_e$. Substituting x/L by r , straight-
 261 forward rearrangements yield:

$$\tilde{\eta}(k_n) = \eta_0 \frac{2L}{R_e} F(a), \quad (25)$$

262 where $a \equiv k_n L$ and:

$$F(a) \equiv 2 \int_0^1 \cos(ar) \eta_*(r) dr. \quad (26)$$

263 Eq. (25) states that the Fourier coefficients of the one-dimensional ice sheet topography (and hence the Fourier coeffi-
 264 cients of the temperature anomalies) are proportional to the horizontal extent in addition to the maximum height. The
 265 two-dimensional Fourier representation of the ice sheet takes the following form:

$$\tilde{\eta}(k_n, l_n) = \eta_0 \frac{A}{R_e^2} F(a) G(b), \quad (27)$$

266 where l_n is the meridional wavenumber, $b \equiv l_n L$, and $G(b)$ is proportional to $F(b)$. Relating the mean height of the ice
 267 sheet to its maximum height as $\eta_m = \gamma \eta_0$, where $0 < \gamma < 1$, Eq. (27) can be rewritten as:

$$\tilde{\eta}(k_n, l_n) = \frac{V}{\gamma R_e^2} F(a) G(b). \quad (28)$$

268 Thus, for any ice sheet representation, the Fourier coefficients of ice sheet topography are proportional to the ice volume
 269 times the functions $F(a)$ and $G(b)$, which are determined by the shape of the ice sheet. Using the first-order plastic
 270 approximation of ice sheet topography, the general formulation of the ice sheet Fourier coefficients can be substituted
 271 by $\gamma = 4(1 + \zeta)/9$ and $\eta_* = \sqrt{1 - x/L}$, implying that:

$$\tilde{\eta}(k_n, l_n) = \frac{9}{4} \frac{V}{R_e^2 (1 + \zeta)} F(a) G(b). \quad (29)$$

272 Using Eq. (18), we can relate the Fourier components of the plastic ice sheet to the corresponding temperature anomalies:

$$\tilde{T} = -\frac{9\mu\chi}{4} \frac{V}{R_e^2 (1 + \zeta)} F(a) G(b), \quad (30)$$

273 where $F(a)$ is now given by:

$$F(a) \equiv 2 \int_0^1 \cos(ar) \sqrt{1 - r} dr. \quad (31)$$

274 This function can be written using the Fresnel integrals C and S as:

$$F(a) = \frac{\sqrt{2\pi}}{a^{3/2}} \left(\sin(a) C \left(\sqrt{\frac{2a}{\pi}} \right) - \cos(a) S \left(\sqrt{\frac{2a}{\pi}} \right) \right), \quad (32)$$

275 where $F(0) = 4/3$. The function F is shown in Fig. 4. For small arguments, the functions F and G decrease only
 276 slowly, implying a regime where the lowest Fourier coefficient of the ice sheet is roughly proportional to V . Specifically,
 277 F decreases only by 3 % in the interval $0 < a < 0.5$. Thus for $a < 0.5$, a linear relationship between the first few

278 Fourier coefficients of the ice sheet and ice volume is a good approximation. At 50° latitude this condition applies when
 279 $L < 2000/n$ km or equivalently when:

$$V < \frac{16(1+\zeta)^{1/2}\sigma^{1/2}}{9} \left(\frac{0.5R_e}{2\pi n} \right)^{5/2}. \quad (33)$$

280 For the parameters given in Table 1 ($\sigma = 10$ m, $\zeta = 0.4$), there is a linear relationship between $\tilde{\eta}$ and V when $V <$
 281 $40 \times 10^6/n^{5/2}$ km³. This is illustrated in Fig. 5: For wavenumber $n = 2$, $\tilde{\eta}$ increases linearly with V until $V = 7.1 \times 10^6$
 282 km³, which is equivalent to $L = 1000$ km. For increasing zonal wavenumbers, the necessary condition for linearity (Eq.
 283 (33)) is strongly constrained by the $n^{-5/2}$ dependence. As a consequence, for $n = 3$ and $n = 4$, the linear relationship
 284 breaks down already at about $V = 2.6 \times 10^6$ km³ ($L = 700$ km) and $V = 1.2 \times 10^6$ km³ ($L = 500$ km), respectively.

285 The properties of the spectral plastic ice sheet representation show that if the response is dominated by a few low
 286 wavenumbers, as suggested in Fig. 2, then the temperature anomaly should initially increase linearly with ice volume.
 287 However, as the ice sheet grows, the increase declines and eventually stops owing to higher values of a and b . This pattern
 288 is analytically described for each Fourier component in Eq. (30), and because the full solution in a linear model is given
 289 by the superposition of the individual Fourier components, it is also evident for all basic states in Fig. 3. Notably, the
 290 present-day basic state temperature anomaly decreases at a slower rate than the other basic states. This occurs because
 291 the strongest response is encountered at higher wavenumbers in the present-day case due to lower value of the zonal
 292 mean wind.

293 THE STATIONARY WAVE INFLUENCE ON THE TEMPERATURE OVER AN 294 EQUATORWARD EXPANDING ICE SHEET

295 In the previous section we showed that if the ice sheet grows, the stationary wave-induced cooling becomes stronger. In
 296 addition, the surface temperature over the ice sheet depends on the latitude as well as on the height of the ice sheet.
 297 Simple one-dimensional models have demonstrated that the general temperature decrease with altitude and latitude
 298 may give rise to two equilibrium solutions: a small unstable ice sheet and a larger stable one (Weertman, 1976). Here,
 299 we follow Roe and Lindzen (2001a) and consider also the effect of stationary wave-induced temperature anomalies on
 300 the mean temperature over the ice sheet. For an anchored northern margin, we write \overline{T}_s , as:

$$\overline{T}_s = T_N - \overline{T}_{ys}L + \Gamma\eta_m + \overline{T}'. \quad (34)$$

301 Our representation of the mean surface temperature over the ice sheet contains the temperature at the northern margin,
 302 T_N , the surface background meridional temperature gradient \overline{T}_{ys} , the lapse rate Γ , and the area-mean stationary wave-
 303 induced temperature \overline{T}' . Both \overline{T}_{ys} and Γ are negative, implying that for a southward expanding ice sheet, there is a

304 warming due to the meridional temperature gradient, and a cooling due to the atmospheric lapse rate. To examine the
 305 different processes contributing to the mean surface temperature change, we differentiate Eq. (34) with respect to V .
 306 Using Eq. (5) for a plastic ice sheet, we obtain:

$$\frac{\partial \bar{T}_s}{\partial V} = -A \bar{T}_{ys} V^{-3/5} + B \Gamma V^{-4/5} + \frac{\partial \bar{T}'}{\partial V}, \quad (35)$$

307 where $A \equiv (2/5)[9/(16(1 + \zeta)^{1/2}\sigma^{1/2})]^{2/5}$ and $B \equiv (4/45)[9\sigma^2/(16(1 + \zeta)^3)]^{1/5}$ are positive constants containing the ice
 308 sheet height-to-length parameter σ and the bedrock sinking parameter ζ . For an equatorward expanding ice sheet,
 309 the background meridional temperature gradient \bar{T}_{ys} (defined negative) leads to a warming over the ice sheet. This
 310 warming is countered by the lapse rate and the stationary waves, both inducing a cooling over the ice sheet. The
 311 relative importance of the processes acting to change the mean temperature depends on the ice volume. The effect
 312 of the elevation (hereafter referred to as the ice-elevation effect) on the mean temperature is strongest for small ice
 313 sheets and decays rapidly with increasing ice volume. The near linear dependence of the stationary wave-temperature
 314 on ice-volume implies a slower decay as the ice volume increases.

315 Figure 6 shows the derivative of the mean temperature with respect to V with and without the effect of the stationary
 316 waves. In the absence of stationary waves, the temperature initially decreases despite the fact that the ice sheet expands
 317 equatorward. The cooling for small ice sheets is related to the ice-elevation effect. The associated reduction of the
 318 ablation can destabilise a small ice sheet, promoting it to expand, as pointed out by Weertman (1976). Eventually, at
 319 about $V = 0.3 \times 10^6 \text{ km}^3$, the effect of the background meridional temperature gradient begins to dominate inducing a
 320 net temperature increase over the expanding ice sheet.

321 The stationary waves induce a mean cooling over the expanding ice sheet (the glacial basic state: solid line in Fig.
 322 3). This is especially true for a range of intermediate sized ice sheets, for which the stationary wave effect is relatively
 323 strong compared to the other processes; There is a regime between about $V = 1 \times 10^6 \text{ km}^3$ and $V = 10 \times 10^6 \text{ km}^3$
 324 (equivalent to $L = 470 \text{ km}$ and $L = 1200 \text{ km}$, respectively), where the cooling due to the stationary waves along with the
 325 ice-elevation almost completely cancel out the effect of the meridional temperature gradient on the mean temperature.

326 For comparison, Fig. 6 illustrates also the stationary wave-parameterisation as suggested by Roe and Lindzen (2001a)
 327 (dashed line). They assumed that the local stationary wave-induced temperature anomaly is proportional to the maxi-
 328 mum height of the ice sheet, i.e. it depends on the ice volume in the same way as the ice-elevation effect. The strength
 329 of the stationary wave-induced cooling in their parameterization is given by $-5^\circ\text{C}/2 \text{ km}$ (equivalent to their CTT case).
 330 Compared to the case without any stationary waves, the inclusion of the stationary wave representation due to Roe and
 331 Lindzen enhances the cooling over the equatorward expanding ice sheet up to one order of magnitude larger ice sheets.
 332 However, this representation of the stationary wave-induced temperature anomaly decays faster with ice volume than

333 our results obtained from the two-level model (illustrated by solid line in Fig. 6). This implies that the representation
334 of Roe and Lindzen shifts into the warming regime for smaller ice sheets.

335 Figure 6 suggests that the stationary waves can strongly modify the mean temperature over an equatorward expanding
336 ice sheet. Potentially, this can result in a strong stationary wave–ablation feedback, especially for small-to-intermediate
337 sized ice sheets. The strength of this feedback, however, is not entirely determined by the area-mean temperature
338 anomaly. Because ablation occurs at the ice sheet margin, the stationary wave feedback depends also on the distribution
339 of the temperature anomaly over the ice sheet. To further examine this issue, one should use a spherical geometry
340 instead of the channel geometry used here.

341 SUMMARY AND CONCLUSION

342 In this study, interactions between the steady atmospheric stationary wave-induced temperature anomalies and ice sheet
343 topography have been considered in a linear quasi-geostrophic two-level model on a β -plane channel. We emphasise that
344 the idealised two-level model neglects several atmospheric processes of importance for the interaction between the
345 stationary waves and ice sheets. For example, we have not considered any interactions between the topography and
346 the mean flow, a feature that could influence also the local atmospheric wave response (Charney and DeVore, 1979).
347 To obtain the qualitative behaviour of the stationary wave-induced temperature response, we chose to monitor the
348 stationary wave feedback using the mean temperature anomaly, averaged over the whole ice sheet area rather than the
349 ice sheet margin. However, the local temperature response in two-level model is quite symmetric around the centre of
350 the ice sheet. Therefore, the qualitative analysis applies also at other parts of the ice sheet like the southern margin. To
351 study the spatial distribution of the temperature anomaly over ice sheet in more detail, it is appropriate to use spherical
352 geometry rather than the channel geometry used here. Furthermore, to allow for physical interpretations and analytical
353 solutions we have used an idealised representation of ice sheet topography, based on the plastic approximation (van der
354 Veen, 1999).

355 The Fourier analysis presented above shows that the ablation due to the stationary wave-induced temperature anoma-
356 lies acts to propagate the ice sheet downstream. This feature was noted by Lindeman and Oerlemans (1987), who
357 investigated mass-balance perturbations on the LGM ice sheets using a two-level atmospheric model in combination
358 with a statistically-based mass-balance model. Further, the positive feedback on the ice sheet due to the ablation
359 anomalies is most pronounced for length scales comparable to that of the stationary Rossby wave; a feature that can
360 be inferred from the equilibrium ice sheet shapes computed by Roe and Lindzen (2001b) with and without the effect of
361 stationary wave induced temperature anomalies. On an infinite ice sheet with constant height, the ablation–stationary
362 wave feedback would act to generate sinusoidal perturbations of a wave length close to that of the stationary wave; and

363 these perturbations would propagate eastward; see Fig. 2. This hypothetical scenario has similarities with the spatial
364 evolution of sea surface temperature anomalies that arises from the interaction with stationary atmospheric waves
365 (Nilsson, 2001). In the coupled atmosphere–ice sheet model of Roe and Lindzen (2001b), the scale-selective stationary
366 wave feedbacks affect how a small initial ice sheet evolves to its equilibrium extent (see their Fig. 13): Initially, the ice
367 sheet expands westward due to topographically-forced accumulation; whereas stationary waves influence the later stages
368 of the evolution, characterized by an eastward expansion of the ice sheet. Ice dynamics plays also an important role for
369 the ice sheet evolution in the simulations of Roe and Lindzen (2001b).

370 A central result in our study is that the area-mean stationary wave-induced cooling over small-to-intermediate sized ice
371 sheets is directly proportional to their ice volume. The underlying reason is that a few low wavenumber stationary waves
372 dominate the response. As long as their wave lengths are large compared to the ice sheet extent, the stationary wave-
373 induced temperature anomaly is proportional to the ice volume. However, the response depends also on the Fourier
374 component of the ice sheet corresponding to the wavenumber of the stationary wave. The amplitude of this Fourier
375 component increases with increasing ice volume. Using the first-order plastic approximation of ice sheet topography,
376 the stationary wave-induced cooling increases linearly with ice volume as long as the dominant wave length of the
377 atmospheric response satisfies the condition $\lambda > 4\pi L$, where L is the half-length of the ice sheet. For an atmospheric
378 response which is dominated by zonal wavenumber 3, we found that $\lambda > 4\pi L$ applies for ice sheets smaller than $L < 700$
379 km, or equivalently $V < 1.5 \times 10^6 \text{ km}^3$ using the standard parameters in this study. For larger ice sheets, the dependence
380 of the local stationary wave-induced cooling on the ice volume becomes gradually weaker, implying that the linear
381 relationship breaks down.

382 The proportionality between the stationary wave-induced temperature and ice volume obtained here is in contrast with
383 Roe and Lindzen (2001a), who parameterised the stationary wave-induced temperature anomaly as being proportional
384 to the maximum height of the ice sheet surface. This representation of the stationary waves gives rise to a relatively
385 strong impact on the mean temperature over small equatorward expanding ice sheets, whereas the representation due to
386 ice volume entails a relatively stronger influence on the mean temperature over larger ice sheets. More specifically, there
387 is a range of intermediate sized ice sheets (here between $V = 1 \times 10^6 \text{ km}^3$ and $V = 10 \times 10^6 \text{ km}^3$) where the stationary
388 waves contribute to a net temperature decrease over an equatorward expanding ice sheet.

389 The amplitude of the topographically-forced stationary wave-induced temperature is a function of the size and shape
390 of the ice sheet as well as the atmospheric basic state. For small changes of the surface zonal wind, we found that
391 the stationary wave-induced temperature anomaly is proportional to $\overline{T}_y L_d$, i.e. the background meridional temperature
392 gradient times the Rossby radius of deformation. Because L_d depends on the atmospheric lapse rate, this result yields

393 an estimate of the impact of the background temperature state on the stationary wave-induced temperature anomaly
394 over the ice sheet. Unfortunately, the changes of the atmospheric basic state through a glacial-interglacial cycle is still
395 an unresolved issue (Abe-Ouchi and others, 2007; Charbit and others, 2007).

396 The present analysis has only considered the stationary wave-interactions with a single isolated ice sheet. The Pleis-
397 tocene glacials, however, have generally been characterised by two continental-scale mid-latitude ice sheets in the
398 Northern Hemisphere. Modelling studies suggest that at LGM, the stationary wave-response to the Laurentide ice
399 sheet enhanced the baroclinic eddy activity downstream, which may lead to an intensification of the storm tracks and
400 the associated precipitation over the Fennoscandian ice sheet (Kageyama and Valdes, 2000). Potentially, the Laurentide
401 ice sheet could also influence the stationary wave-induced ablation on Fennoscandia. However, the far-field stationary
402 wave-response is not as strong as the local response (Held, 1983), suggesting that tele-connection effect presumably are
403 small compared to effects of stationary waves forced locally by the Fennoscandian ice sheet.

404 In agreement with Lindeman and Oerlemans (1987) and Roe and Lindzen (2001b), we found that the atmospheric flow
405 response has a leading order impact on the local climate over ice sheets, manifested by negative temperature anomalies
406 of several degrees. The new important result is that the stationary wave-induced cooling locally over the ice sheet is
407 proportional to the ice volume and the product of the meridional temperature gradient times the Rossby radius of
408 deformation. These intriguing new features deserve further attention in more realistic framework that includes a more
409 complete atmospheric model and a dynamical representation of the ice sheet.

410 ACKNOWLEDGEMENTS

411 We thank Florence Colleoni, Nina Kirchner, Erland Källén, Andreas Vallgren and two anonymous reviewers for their
412 valuable comments on the manuscript. The work reported here was supported by the Swedish Research Council and
413 the Climate Research School at Stockholm University and is a contribution from the Bert Bolin Centre for Climate
414 Research.

415 REFERENCES

- 416 Abe-Ouchi, A., T. Segawa and F. Saito, 2007. Climatic conditions for modelling the Northern Hemisphere ice sheets throughout
417 the ice age cycle, *Clim. Past*, **3**, 423–438.
- 418 Berger, A., 1978. Long-term variations of caloric insolation resulting from the Earth's orbital elements, *Quat. Res.*, **9**, 139–167.
- 419 Bonelli, S., S. Charbit, M. Kageyama, M.-N. Woillez, G. Ramstein, C. Dumas and A. Quiquet, 2009. Investigating the evolution
420 of major Northern Hemisphere ice sheets during the last glacial-interglacial cycle, *Clim. Past*, **5**, 329–345.

421 Charbit, S., C. Ritz, G. Philippon, V. Peyaud and M. Kageyama, 2007. Numerical reconstructions of the Northern Hemisphere
422 ice sheets through the last glacial-interglacial cycle, *Clim. Past*, **3**, 15–37.

423 Charney, J. G. and J. G. DeVore, 1979. Multiple flow equilibria in the atmosphere and blocking, *J. Atmos. Sci.*, **36**, 1205–1216.

424 Charney, J. G. and A. Eliassen, 1949. A numerical method for predicting the perturbations of the middle latitude westerlies,
425 *Tellus*, **1**, 38–54.

426 Clark, P. U. and A. C. Mix, 2002. Ice sheet and sea level of the last glacial maximum, *Quat. Sci. Rev.*, **21**, 1–7.

427 Cook, K. H. and I. M. Held, 1988. Stationary waves of the ice age climate, *J. Climate*, **1**, 807–819.

428 Cubasch, U., E. Zorita, F. Kaspar, J. F. Gonzalez-Rouco, H. von Storch and K. Prömmel, 2006. Simulation of the role of solar
429 and orbital forcing on climate, *Advances in Space Research*, **37**, 1629–1634.

430 Dyke, A. S., 2004. An outline of North American deglaciation with emphasis on central and northern Canada, Ehlers, J. and
431 P. L. Gibbard, eds., *Quaternary Glaciations-Extent and Chronology, Part II*, Elsevier, vol. 2b, 373–424.

432 Dyke, A. S., J. T. Andrews, P. U. Clark, J. H. England, G. H. Miller, J. Shaw and J. J. Veillette, 2002. The Laurentide and
433 Inuitian ice sheets during the Last Glacial Maximum, *Quat. Sci. Rev.*, **21**(1-3), 9 – 31.

434 Hall, M. N. J., P. J. Valdes and B. Dong, 1996. The maintenance of the last great ice sheets: A UGAMP GCM study, *J. Climate*,
435 **9**, 1004–1019.

436 Held, I. M., 1983. Stationary and quasi-stationary eddies in the extratropical troposphere: Theory, Hoskins, B.J. and R.F. Pearce,
437 eds., *Large-scale dynamical processes in the atmosphere*, Academic Press, 127–169.

438 Holton, J. R., 2004. *An introduction to dynamic meteorology*, Elsevier Academic Press.

439 Hoskins, B. J. and D. J. Karoly, 1981. The steady linear response of a spherical atmosphere to thermal and orographic forcing,
440 *J. Atmos. Sci.*, **38**, 1179–1196.

441 Justino, F., A. Timmermann, U. Merkel and E. P. Souza, 2005. Synoptic reorganization of atmospheric flow during the last glacial
442 maximum, *J. Climate*, **18**, 2826–2845.

443 Kageyama, M., S. Charbit, C. Ritz, M. Khodri and G. Ramstein, 2004. Quantifying ice-sheet feedbacks during the last glacial
444 inception, *Geophys. Res. Lett.*, **31**, L24203, DOI: 10.1029/2004GL021339.

445 Kageyama, M and P. J. Valdes, 2000. Impact of the North American ice-sheet orography on the Last Glacial Maximum eddies
446 and snowfall, *Geophys. Res. Lett.*, **27**(10), 1515–1518.

447 Källén, E., C. Crafoord and M. Ghil, 1979. Free oscillations in a climate model with ice-sheet dynamics, *J. Climate*, **36**, 2292–2303.

448 Kleman, J., J. Fastook and A. P. Stroeven, 2002. Geologically and geomorphologically constrained numerical model of Laurentide
449 ice sheet inception and build-up, *Quat. Int.*, **95-6**, 87–98.

450 Kutzbach, J. E. and P. J. Guetter, 1986. The influence of changing orbital parameters and surface boundary conditions on
451 simulations for the last 18 000 years, *J. Atmos. Sci.*, **43**, 1726–1759.

452 Lindeman, M. and J. Oerlemans, 1987. Northern Hemisphere ice sheets and planetary waves: a strong feedback mechanism, *J.*
453 *Climatology*, **7**, 109–117.

454 Milankovitch, M., 1930. Mathematische klimalehre und astronomische theorie der klimaschwankungen I, Köppen, W. and
455 R. Geiger, eds., Handbuch der klimatologie, Part A, Gebruder Borntraeger, Berlin.

456 Nilsson, J., 2001. Spatial reorganization of SST anomalies by stationary atmospheric waves, *Dyn. Atmos. Oce.*, **34**, 1–21.

457 Oerlemans, J., 1979. A model of a stochastically driven ice sheet with planetary wave feedback, *Tellus*, **31**, 469–477.

458 Oerlemans, J., 1980. Model experiments on the 100,000-yr glacial cycle, *Nature*, **287**, 430–432.

459 Otieno, F. O. and D. H. Bromwich, 2009. Contribution of atmospheric circulation to inception of the Laurentide ice sheet at 116
460 kyr BP, *J. Climate*, **22**, 39–57.

461 Paillard, D., 1998. The timing of Pleistocene glaciations from a simple multiple-state climate model, *Nature*, **391**, 378–381.

462 Peixoto, J. P. and A. Oort, 1992. The physics of climate, Springer-Verlag.

463 Pollard, D., 1982. A simple ice sheet model yields realistic 100 kyr glacial cycles, *Nature*, **296**, 334–338.

464 Roe, G. H., 2005. Orographic precipitation, *Ann. Rev. Earth Planet. Sci.*, **33**, 645–671.

465 Roe, G. H. and R. S. Lindzen, 2001a. A one-dimensional model for the interaction between continental-scale ice sheets and
466 atmospheric stationary waves, *Clim. Dyn.*, **17**, 479–487.

467 Roe, G. H. and R. S. Lindzen, 2001b. The mutual interaction between continental-scale ice sheets and atmospheric stationary
468 waves, *J. Climate*, **14**, 1450–1465.

469 Sanberg, J. A. M. and J. Oerlemans, 1983. Modeling of Pleistocene European ice sheets: the effect of upslope precipitation, *Geol.*
470 *Mijnbouw*, **62**, 267–273.

471 Stone, P., 1978. Baroclinic adjustment, *J. Atmos. Sci.*, **35**, 561–571.

472 Tarasov, L. and W. R. Peltier, 1997. Terminating the 100 kyr cycle, *J. Geophys. Res.*, **102**, 21665–21693.

473 Tarasov, L. and W. R. Peltier, 2004. A geophysically constrained large ensemble analysis of the deglacial history of the North
474 American ice-sheet complex., *Quat. Sci. Rev.*, **23**, 359–388.

475 van den Berg, J., R. van de Wal and J. Oerlemans, 2008. Mass balance model for the Eurasian ice sheet for the last 120,000 years,
476 *Global Planet. Change*, **61**, 194–208.

477 van der Veen, C. J., 1999. Fundamentals of glacier dynamics, A.A.Balkema.

478 Weertman, J., 1976. Milankovitch solar radiation variations and ice age ice sheet sizes, *Nature*, **261**, 17–20.

To relate the stationary wave-induced temperature anomaly to ice sheet topography, we insert Eq. (17) into Eqs. (11) and (12), and multiply by i/k :

$$\tilde{\psi}_M = -\tilde{\psi}_T \left(\frac{\gamma_{MM}}{\gamma_{MT}} + i \frac{R_T}{\gamma_{MT}} \right) \quad (\text{A1})$$

$$\tilde{\psi}_T = -\frac{2f_0}{H} (U_M - U_T) \chi \tilde{\eta}, \quad (\text{A2})$$

where:

$$\chi \equiv \left(\frac{\chi_\gamma}{\chi_\gamma^2 + \chi_R^2} - i \frac{\chi_R}{\chi_\gamma^2 + \chi_R^2} \right), \quad (\text{A3})$$

$$\chi_\gamma \equiv \gamma_{TM} + \frac{\gamma_{MM}}{\gamma_{MT}} \gamma_{TT} + \frac{R_F R_T}{\gamma_{MT}}, \quad (\text{A4})$$

$$\chi_R \equiv R_T \left(1 + \frac{\gamma_{TT}}{\gamma_{MT}} \right) - R_F \left(1 + \frac{\gamma_{MM}}{\gamma_{MT}} \right) \quad (\text{A5})$$

$$\gamma_{MM} \equiv K^2 (U_M + U_T) - \beta_0 + 2U_M L_d^{-2}, \quad (\text{A6})$$

$$\gamma_{MT} \equiv K^2 (U_M + U_T) - \beta_0 - 2U_T L_d^{-2}, \quad (\text{A7})$$

$$\gamma_{TM} \equiv K^2 (U_M - U_T) - \beta_0 + 2U_M L_d^{-2}, \quad (\text{A8})$$

$$\gamma_{TT} \equiv K^2 (U_M - U_T) - \beta_0 + 2U_T L_d^{-2}, \quad (\text{A9})$$

$$R_T \equiv \frac{2}{\tau_T L_d^2 k}, \quad (\text{A10})$$

$$R_F \equiv \frac{K^2}{\tau_F k}. \quad (\text{A11})$$

480 Using the hydrostatic equation Eq. (13), the spectral representation of stationary wave-induced temperature anomaly
481 yields:

$$\tilde{T} = -\mu \chi \tilde{\eta}. \quad (\text{A12})$$

Table 1. Numerical values of the parameters used in this study.

Quantity	Parameter	Value
Coriolis parameter	f_0	$1.1 \times 10^{-4} \text{ s}^{-1}$
Meridional gradient of f_0	β_0	$1.5 \times 10^{-11} \text{ (ms)}^{-1}$
Geometric model depth	H	12 km
Radiative damping time-scale	τ_T	10 days
Ekman damping time-scale	τ_F	5 days
Ice sheet northern margin	y_N	75°N
Plastic ice sheet parameter	σ	10 m
Bedrock depression parameter	ζ	0.4
Gas constant for dry air	R	$287 \text{ J K}^{-1} \text{ kg}^{-1}$

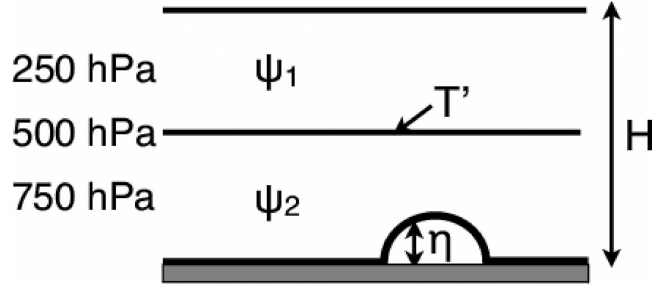


Fig. 1. The two-level model configuration. The stream function anomalies ψ_1 and ψ_2 correspond to the 250 hPa and 750 hPa levels, respectively. The barotropic and baroclinic stream function anomalies ψ_M and ψ_T are given by $\psi_M = (\psi_1 + \psi_2)/2$ and $\psi_T = (\psi_1 - \psi_2)/2$. The temperature anomaly 500 hPa, T' , is proportional ψ_T , and the topographic forcing is represented by the height of the ice sheet surface, η .

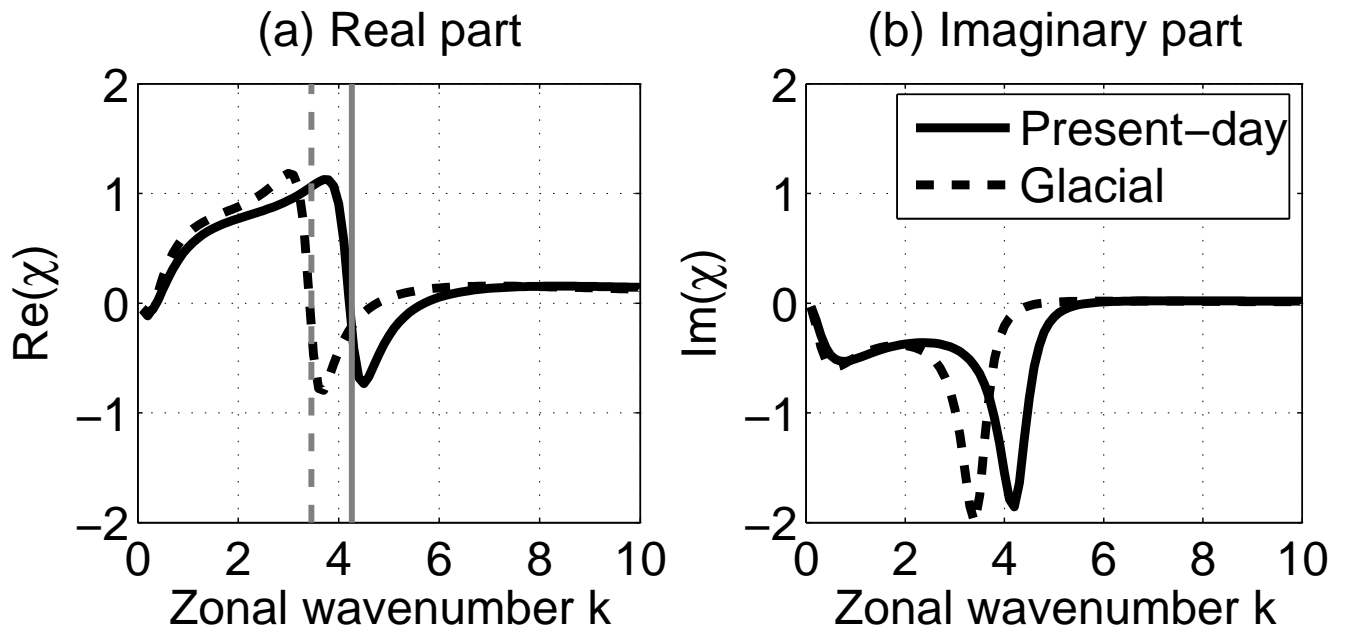


Fig. 2. The (a) real and (b) imaginary parts of the transfer function χ (cf. Eq. (18)) for the following atmospheric basic states: "Present-day" (solid line; $U_M = 9 \text{ m s}^{-1}$, $U_T = 3.6 \text{ m s}^{-1}$ and $L_d = 700 \text{ km}$) and "glacial" (dashed line; $U_M = 12 \text{ m s}^{-1}$, $U_T = 4.8 \text{ m s}^{-1}$ and $L_d = 810 \text{ km}$) as a function of zonal wavenumber k (meridional wavenumber is set to $l = 1$). The stationary Rossby wavenumbers, k_s , for the present-day and glacial basic states are featured by the grey vertical solid and dashed lines, respectively. The values of χ are set non-dimensional by the scale factor $U_M L_d^{-2}$. $\text{Re}(\chi) < 0$ corresponds to a positive stationary wave-induced temperature anomaly over the ice sheet, and $\text{Im}(\chi) < 0$ implies a positive phase speed (i.e. eastward ice sheet propagation).

Temperature anomaly vs. ice volume

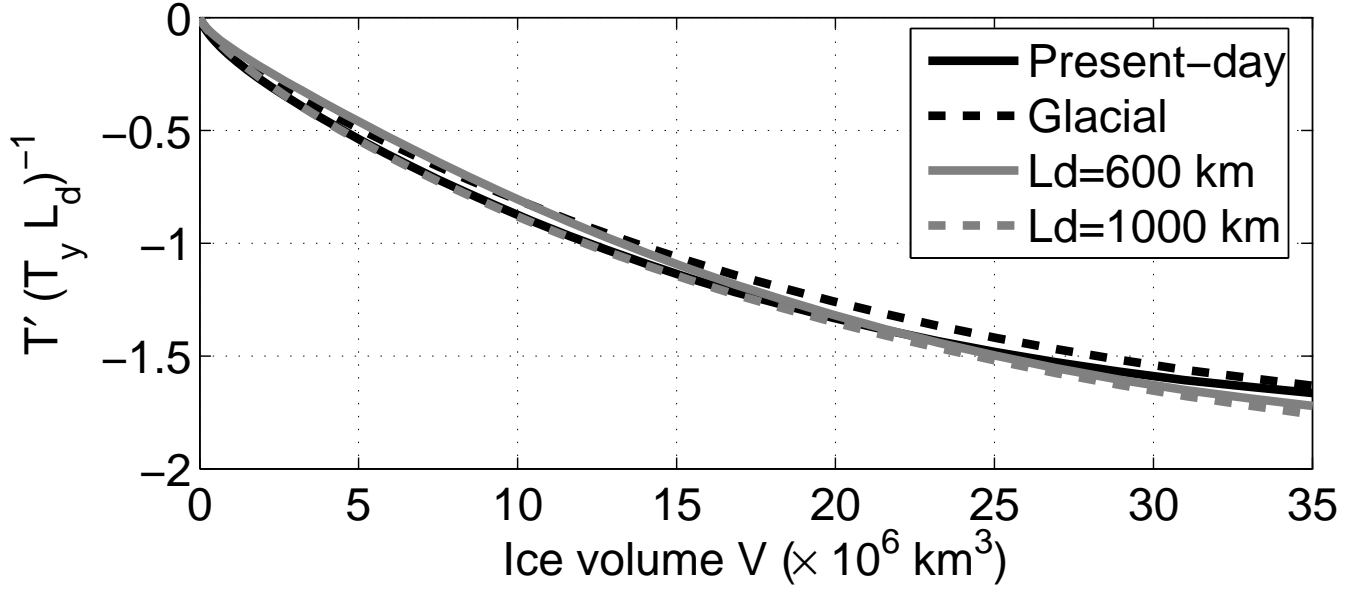


Fig. 3. The scaled area-mean stationary wave-induced temperature anomaly $\overline{T}' (\overline{T}_y L_d)^{-1}$ as a function of ice volume V for the following atmospheric basic states: "Present-day" (solid line; $U_M = 9 \text{ m s}^{-1}$, $U_T = 3.6 \text{ m s}^{-1}$ and $L_d = 700 \text{ km}$) and "glacial" (dashed line; $U_M = 12 \text{ m s}^{-1}$, $U_T = 4.8 \text{ m s}^{-1}$ and $L_d = 810 \text{ km}$). The grey lines represent the same basic state as "glacial", with the exception that $L_d = 600 \text{ km}$ (solid gray line) and $L_d = 1000 \text{ km}$ (dashed gray line). These states are included to illustrate the sensitivity of the stationary temperature anomaly to changes in the atmospheric lapse rate.

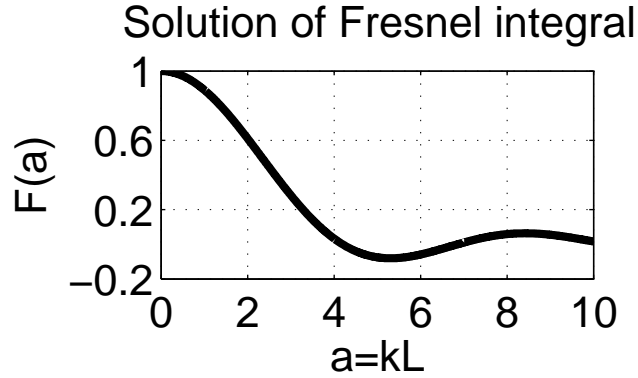


Fig. 4. Solution of the Fresnel integral defined in Eq. (32). The parameter a is given by $a = kL$, where k is the zonal wavenumber and L is the ice sheet half-length. When $a < 0.5$, the value of $F(a)$ changes only about 3 %, implying a close to linear relationship between the Fourier amplitudes of ice sheet topography and ice volume.

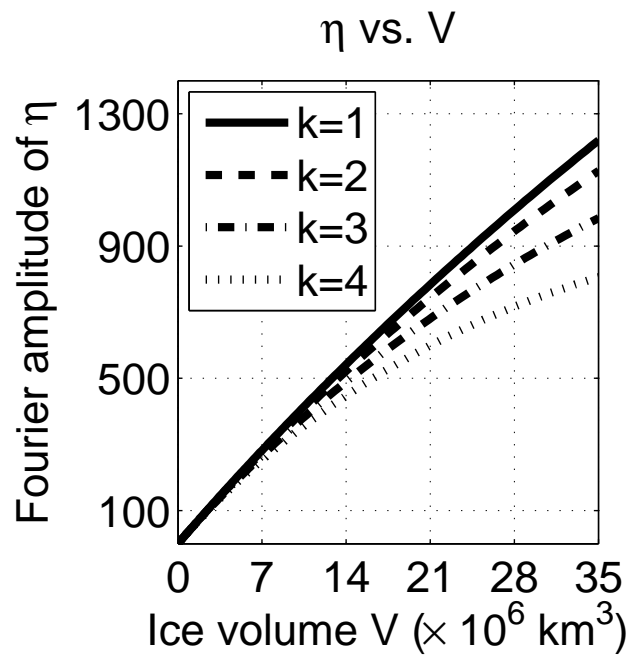


Fig. 5. The amplitude of the Fourier coefficients of ice sheet topography $\tilde{\eta}$ as a function of ice sheet volume V for zonal wavenumber $k = 1$ (solid line), $k = 2$ (dashed line), $k = 3$ (dashed-dotted line), and $k = 4$ (dotted line). All solutions have been calculated using meridional wavenumber $l = 1$.

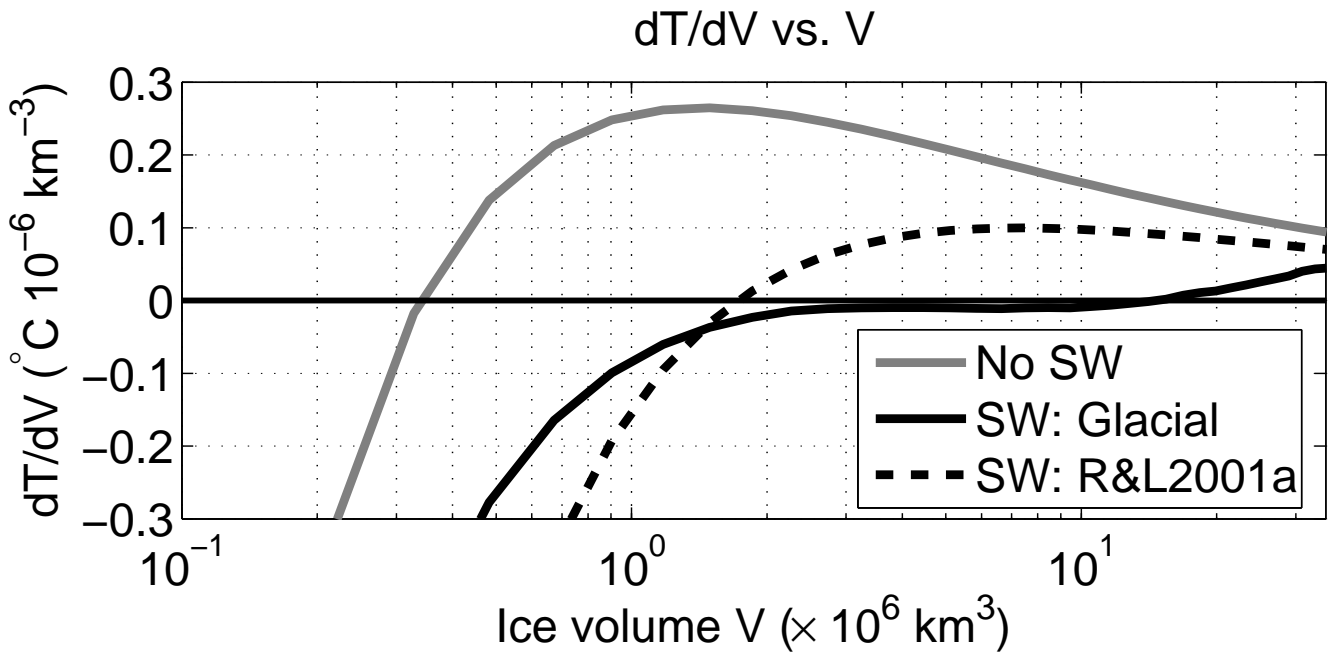


Fig. 6. The derivative of the mean surface temperature over the ice sheet with respect to ice volume (i.e. the solution of Eq. (35)) in the absence of stationary waves (gray line), and with the stationary waves (black lines). The black solid line represents the case when the stationary wave-induced temperature anomaly computed in the two-level model with the "glacial" basic state: ($U_M = 12$ m s $^{-1}$, $U_T = 4.8$ m s $^{-1}$ and $L_d = 810$ km). The black dashed line is calculated using the stationary wave-induced temperature representation given by Roe and Lindzen (2001a). The surface meridional temperature gradient is set to $-7^\circ\text{C} (1000) \text{ km}^{-1}$ and the atmospheric lapse rate to $\Gamma = -6.5^\circ\text{C km}^{-1}$.